Two-dimensional effects in Josephson junctions: Static properties

Jean-Guy Caputo,[1,2] Nikos Flytzanis,[2] Yuri Gaididei,[2,3] and Emmanuel Vavalis[4]
[1]*Laboratoire de Mathématiques, INSA and URA CNRS 1378, BP8, 76131 Mont-Saint-Aignan Cedex, France*
[2]*Physics Department, University of Crete, 71409 Heraklion, Greece*
[3]*Institute for Theoretical Physics, 252143 Kiev, Ukraine*
[4]*Mathematics Department, University of Crete, 71409 Heraklion, Greece and IACM, FORTH, Heraklion, Greece*
(Received 14 June 1995; revised manuscript received 10 April 1996)

We studied the dependence of the maximum tunneling current on external magnetic field for large area Josephson junctions with overlap boundary conditions. We used direct numerical solutions and developed a split Fourier mode method to study the electromagnetic behavior. The steady-state pattern consists of two terms, the first of which satisfies the in-line-like bias current boundary conditions and has zero fluxon content. The second is treated in a mode expansion in the y direction and only two terms are sufficient to reproduce the direct solution of the two-dimensional junction for widths up to 2π times the Josephson characteristic length. [S1063-651X(96)08007-5]

PACS number(s): 02.70.−c, 03.40.Kf, 74.50.+r

I. INTRODUCTION

The maximum tunneling current $I_{\max}$ through a Josephson junction depends on the strength of the external magnetic field, the junction geometry, and the type of boundary conditions [1]. Here, for simplicity we will consider rectangular junctions of length L and width W, which can be classified as (a) short if $L,W \ll \lambda_J$, (b) long if $L \gg \lambda_J \gg W$, or (c) large if $L,W > \lambda_J$. The parameter λ_J is the Josephson penetration depth, i.e., a characteristic length over which magnetic flux variation occurs in the junction. It depends on the critical tunneling current density J_0 as the inverse of the square root. In general $L,W,\lambda_J \gg d_0,\lambda_L$, where d_0 is the oxide thickness in the barrier and λ_L is the London penetration depth in the superconducting films.

For small dimensions and/or low critical current densities, the magnetic field produced by the junction can be neglected and the external field dependence of $I_{\max}$ gives the well known Fraunhofer-like diffraction pattern [2–4] for a uniform critical current density J_0. For a given shape of the junction the $I_{\max}$ vs H patterns are rather insensitive to various electrode configurations (reflected in the boundary conditions) as long as the junction dimensions are less than λ_J.

For large current densities or $L > \lambda_J$ the self-field created by the junction current influences strongly the field dependence of $I_{\max}$ according to the ratio L/λ_J. For large length the junction exhibits a Meissner-like effect screening weak external magnetic fields to within the Josephson penetration length λ_J from the edges, due to internal currents [5–8]. For increasing external magnetic field, the junction behaves as a nonuniform one.

In some technological applications one must consider large area junctions, whose electromagnetic behavior is strongly affected by geometrical factors and boundary conditions. Even for narrow junctions it is useful to estimate the effect of the width. The perimeter of a junction always has a degree of nonuniformity which can increase with time (if the perimeter is exposed). Its effect (not easily estimated) is much more important in a narrow junction than in a wide junction, since the percentage of size of inhomogeneity is greatly reduced. It is also easier to pattern a specific profile for a variable width when the average junction width is not small. An interesting application for a wide junction is for nuclear radiation detection [14], making use at one end of the shaping of the junction as a wedge so that fluxons created are directed and transmitted to an attached transmission line and the detector is returned to its equilibrium state. Thus the understanding of large junction electrodynamics is important also for device applications. Due to the lack of analytic solutions [unlike the one-dimensional (1D) case], the direct numerical determination of the magnetic flux patterns is computationally intensive. Thus an approximate approach to the problem of current flow in junctions of various geometries has been discussed [9,10]. It uses a piecewise linear current phase relationship, i.e., $J_z \sim \Phi$ (instead of the Josephson relation), where Φ is the phase difference of the superconducting order parameters in the superconducting films. While the model does not reproduce all the features of the spatial variation of $\Phi(x,y)$ it can give some integrated properties and indications for the behavior for various geometries.

The various boundary conditions, in addition to determining the spatial patterns for the constant phase lines, can also influence some important parameters such as the maximum tunneling current. In calculations the simplest boundary conditions are those due to the in-line geometry where the pattern is one-dimensional even for a wide junction. The numerical procedure developed in [6] provides the dependence of $I_{\max}$ on H for arbitrary length. The overlap geometry, on the other hand, introduces two-dimensional patterns, when both external current and magnetic field are applied. For overlap narrow junctions ($W \ll \lambda_J \ll L$) one can develop an effective one-dimensional model where the magnetic field enters as a boundary condition on a perturbed sine-Gordon equation, with the external current acting as driving term [11].

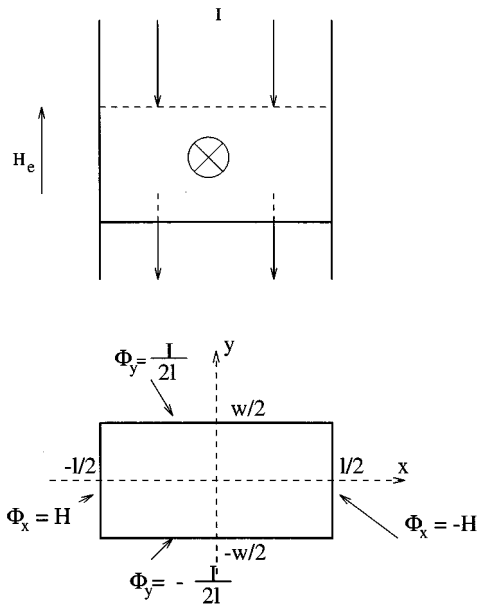

FIG. 1. (a) Schematic diagram (top) of the overlap large Josephson junction. The current from the upper electrode goes through the junction and comes in the lower electrode. (b) Overlap boundary conditions for the 2D static sine-Gordon equation (bottom).

In this paper we present a split Fourier mode (SFM) expansion method which, without increase in computational effort, can accurately describe the static properties of a relatively wide ($W/\lambda_J<2\pi$) junction. In fact, it gives good agreement with the results of direct numerical solution (also presented here) of the two-dimensional problem with the overlap boundary conditions. The procedure gives the possibility to study even very wide junctions by including several terms in the expansion.

In Sec. II we present the split Fourier mode method which captures the dominant variations in the x and y directions that are caused by the magnetic field and the external current, respectively. The coupling between x and y is treated in a mode expansion. In Sec. III we derive a reduced model where only two modes are kept, transforming thus the 2D partial differential equation (PDE) problem to the solution of a system of three ordinary differential equation (ODE) problems, one of which is uncoupled. In Sec. IV we discuss the magnetic flux and introduce the notion of x- and y- direction fluxon content. In Sec. V we present the numerical results and compare them with the direct solution of the 2D problem, and in the final section we summarize our results.

II. 2D MODEL

We consider a two-dimensional Josephson junction which consists of two superconducting metal plates (parallel to the x-y plane) separated by a thin oxide layer [Fig. 1(a)]. The electromagnetic behavior of such a system is governed by Maxwell's equations coupled with the Josephson equation

$$J_z(x,y)=J_0\sin\Phi(x,y) \tag{1}$$

for the tunneling supercurrent density through the oxide layer. In Eq. (1) $\Phi(x,y)$ is the phase difference of the order parameters in the two superconductors, and the constant J_0 is the maximum Josephson current density. In general J_0 depends on material and geometry parameters and can be space dependent.

If the thickness d_0 of the oxide layer is small as compared with the London penetration depths in the two superconducting films λ_1 and λ_2, a two-dimensional approach to this problem is quite satisfactory [1] and it can be reduced to the two-dimensional sine-Gordon equation

$$-\Phi_{tt}+\nabla^2\Phi=\sin\Phi+\beta\Phi_t, \tag{2}$$

where the unit of length is the Josephson penetration length $\lambda_J=\sqrt{\hbar/2J_0\mu_0 d}$, with $d=\lambda_1+\lambda_2+d_0$ and μ_0 the permeability of vacuum. The unit of time is the inverse of the plasma frequency $\omega_p=(2eJ_0/\hbar C)^{1/2}$, C being a capacity between superconducting layers. The last term in the right-hand side of Eq. (2) represents dissipative effects due to quasiparticle tunneling with the McCumber parameter $\beta=(\hbar/2eRJ_0)\omega_p$, where R is an effective normal resistance. In the following all lengths are scaled to λ_J so that the junction dimensions are $\ell=L/\lambda_J$, $w=W/\lambda_J$, while we also define dimensionless magnetic field and current correspondingly as

$$\mathcal{H}_e=\frac{2\mu_0 ed\lambda_J}{\hbar}H_e, \quad \mathcal{I}=\frac{2\mu_0 ed}{\hbar}I.$$

The relation between the effective magnetic field $\vec{\mathcal{H}}$ and the phase difference Φ is given by

$$\vec{\mathcal{H}}=-(\hat{z}\times\vec{\nabla}\Phi), \tag{3}$$

where $\hat{z}$ is the unit vector normal to the junction plane.

The boundary conditions for Eq. (2) are obtained from Eq. (3) and have the form

$$\vec{n}\cdot\vec{\nabla}\Phi|_C=\vec{n}\cdot[\hat{z}\times(\vec{\mathcal{H}}_e+\vec{\mathcal{H}}_I)]|_C, \tag{4}$$

where $\vec{n}$ is the outward normal to the boundary of the junction region C. In Eq. (4) $\vec{\mathcal{H}}_e$ is an external dimensionless magnetic field and $\vec{\mathcal{H}}_I$ is the magnetic field caused by a current passing through the junction. In what follows the external magnetic field $\vec{\mathcal{H}}_e$ is assumed to be directed along the y axis. In the case of a rectangular junction [Fig. 1(a)] of normalized length ℓ and width w ($\ell>w$), the boundary conditions (4) for the overlap geometry may be written [10] in the form

$$\left.\frac{\partial\Phi}{\partial x}\right|_{x=\pm\ell/2}=\mathcal{H}_e, \tag{5a}$$

$$\left.\frac{\partial\Phi}{\partial y}\right|_{y=\pm w/2}=\pm\frac{\mathcal{I}}{2\ell}, \tag{5b}$$

where $\mathcal{I}$ is the normalized total bias current through the junction. In Fig. 1(b) we show the boundary conditions for the 2D equation for $\Phi(x,y)$ corresponding to the overlap geometry.

In the general case Eq. (2) under the boundary conditions (5) can only be solved numerically. At the same time the

inequality $w \ll \ell$ in the case of a narrow junction suggests separating transversal and longitudinal modes and using a Galerkin-type method to solve the problem. To this end we first consider the auxiliary problem of the 1D Josephson junction

$$\frac{d^2\Phi_0(y)}{dy^2} = \sin\Phi_0(y), \tag{6}$$

with the in-line boundary condition at zero external magnetic field, i.e.,

$$\left.\frac{d\Phi_0}{dy}\right|_{y=\pm w/2} = \pm\frac{\mathcal{I}}{2\ell}. \tag{7}$$

The solution of this problem is well known (see Refs. [1,6]) and can be expressed in terms of Jacobi elliptic functions as

$$\sin\Phi_0 = 2\sqrt{m m_1}\,\mathrm{cd}(y|m)\,\mathrm{nd}(y|m), \tag{8}$$

$$\frac{d\Phi_0}{dy} = 2\sqrt{m m_1}\,\mathrm{sd}(y|m), \tag{9}$$

where $\mathrm{pq}(y|m)$ with (p,q=s, c, d, n) are Jacobi elliptic functions with modulus m ($m_1 = 1-m$ is the complementary modulus) [12]. The period of the solution is $4K(m)$, where $K(m)$ is the complete elliptic integral of the first kind. The modulus m can be obtained from the boundary condition (7)

$$2\sqrt{m m_1}\,\mathrm{sd}\left(\frac{w}{2}\middle| m\right) = \frac{\mathcal{I}}{2\ell}. \tag{10}$$

If m is close to unity Eq. (10) simplifies to

$$m \approx 1 - \left(\frac{\mathcal{I}}{2\ell}\right)^2 \frac{1}{4}\,\frac{1}{\sinh^2(w/2)}.$$

Now, a solution of the form

$$\Phi(x,y,t) = \Phi_0(y) + \Psi(x,y,t) \tag{11}$$

reduces Eqs. (2) and (5) to

$$-\Psi_{tt} - \beta\Psi_t + \nabla^2\Psi = \sin[\Phi_0(y) + \Psi(x,y)] - \sin[\Phi_0(y)], \tag{12}$$

$$\left.\frac{\partial\Psi}{\partial x}\right|_{x=\pm\ell/2} = \mathcal{H}_e, \tag{13a}$$

$$\left.\frac{\partial\Psi}{\partial y}\right|_{y=\pm w/2} = 0. \tag{13b}$$

The solution of Eq. (2) under the boundary conditions (5) must be a symmetric function of the transversal variable y. It can be shown that the function $\Psi(x,y,t)$ from Eq. (11) must also be symmetric in y due to the symmetry of the boundary conditions. Therefore taking into account the boundary conditions (13a) we can represent the function $\Psi(x,y,t)$ by a Fourier series which satisfies the boundary condition (13b),

$$\Psi(x,y,t) = \sum_{n=0}^{\infty} A_n(x,t)\cos\frac{2\pi n y}{w}, \tag{14}$$

where the coefficients $A_n(x,t)$ are determined by the usual projection. Substituting Eq. (14) into Eqs. (12) and (13b) and using the notation $\partial_x \equiv \partial/\partial x$ we get

$$\begin{aligned} -\partial_t^2 A_n(x,t) - \beta\partial_t A_n(x,t) + \partial_x^2 A_n(x,t) - \left(\frac{2\pi n}{w}\right)^2 A_n(x) \\ = \frac{2-\delta_{n0}}{w}\int_{-w/2}^{w/2} dy\,\cos\frac{2\pi n y}{w}\left\{\sin\left[\Phi_0(y) + \sum_{n=0}^{\infty} A_n(x,t)\cos\frac{2\pi n y}{w}\right] - \sin\Phi_0(y)\right\}, \end{aligned} \tag{15}$$

$$\partial_x A_n\left(\pm\frac{\ell}{2}, t\right) = \delta_{n0}\mathcal{H}_e, \quad n = 0,1,2,\ldots, \tag{16}$$

where $\delta_{nn'}$ is the Kronecker delta.

It is interesting to remark here that in the absence of dissipation ($\beta = 0$) Eqs. (15) and (16) can be obtained by minimizing the Lagrangian functional

$$\begin{aligned} E = \int_{-\ell/2}^{\ell/2} dx\left\{\sum_n \left[\frac{1+\delta_{no}}{4}[-(\partial_t A_n)^2 + (\partial_x A_n)^2] + \left(\frac{\pi n}{w}\right)^2 A_n^2 - S_n A_n\right] \right. \\ \left. + 2\mathcal{H}_e A_0(x)\left[\delta\left(x+\frac{\ell}{2}\right) - \delta\left(x-\frac{\ell}{2}\right)\right] - F(\{A_n\})\right\}, \end{aligned} \tag{17}$$

where

$$F(\{A_n\}) = \frac{1}{w}\int_{-w/2}^{w/2} dy\,\cos\left[\Phi_0(y) + \sum_{n=0}^{\infty} A_n(x,t)\cos\frac{2\pi n y}{w}\right] \tag{18}$$

and where the abbreviation

$$S_n = \frac{1}{w}\int_{-w/2}^{w/2} dy\,\sin[\Phi_0(y)]\cos\frac{2\pi n y}{w} \tag{19}$$

was used.

It is seen from Eq. (15) that only the modes with $n \leq N \equiv [w/2\pi]$ ($[x]$ is the integer part of the number x) have an influence on the properties of the junction. The modes with large n give contributions which decrease as n^{-2}. In what follows we will consider the properties of not very wide junctions and will assume that $w \leq 2\pi$. Thus we can neglect all modes with $n \geq 2$ and take into account only the modes with $n = 0$ and $n = 1$. Moreover, when $w < 2\pi$ we have $A_1(x,t) < A_0(x,t)$. Therefore we shall neglect effects caused by nonlinear interactions of the $n = 1$ mode and will take into account nonlinear properties of the mode $n = 0$ as well as the coupling between both these modes. This allows us to write Eq. (18) as

$$F(A_0,A_1)=\frac{1}{w}\int_{-w/2}^{w/2}dy\ \cos\left(\Phi_0(y)+A_0+A_1\cos\frac{2\pi y}{w}\right)$$
$$\approx -C_0\cos A_0+S_0\sin A_0+(S_1\cos A_0+C_1\sin A_0)A_1+\frac{1}{2}(C_2\cos A_0-S_2\sin A_0)A_1^2, \quad (20)$$

where

$$C_n=\frac{1}{w}\int_{-w/2}^{w/2}dy\ \cos[\Phi_0(y)]\cos\frac{2\pi n y}{w}. \quad (21)$$

From Eqs. (15), (17), and (20) we obtain that the amplitudes $A_0(x,t)$ and $A_1(x,t)$ are governed by the equations

$$-\partial_t^2A_0-\beta\partial_tA_0+\partial_x^2A_0=C_0\sin A_0+S_0\cos A_0+(C_1\cos A_0-S_1\sin A_0)A_1-\frac{1}{2}(C_2\sin A_0+S_2\cos A_0)A_1^2-S_0, \quad (22)$$

$$-\partial_t^2A_1-\beta\partial_tA_1+\partial_x^2A_1=\left(\frac{2\pi}{w}\right)^2A_1+2[C_1\sin A_0+S_1\cos A_0+(C_2\cos A_0-S_2\sin A_0)A_1-S_1], \quad (23)$$

under the boundary conditions

$$\partial_xA_0(x,t)|_{x=\pm\ell/2}=\mathcal{H}_e, \quad (24a)$$

$$\partial_xA_1(x,t)|_{x=\pm\ell/2}=0. \quad (24b)$$

Equations (22)–(24) give an effective description of the electrodynamics of a long overlap geometry Josephson junction. It is worth noticing that to describe static and dynamic properties for the overlap boundary conditions a perturbed one-dimensional sine-Gordon equation has been used in the form

$$\Phi_{xx}-\Phi_{tt}=\sin\Phi+\beta\Phi_t-\frac{\mathcal{I}}{J_0\ell w}. \quad (25)$$

Eilbeck *et al.* in Ref. [13] represented a solution of Eq. (2) in the form (11) with $\Phi_0(y)=(\mathcal{I}/\ell wJ_0)(y^2/2)$ and assuming that $(1/8)(\mathcal{I}w/J_0\ell)\ll 1$ they derived the effective equation (25). In a recent paper Pagano *et al.* [14] proposed an approximate averaging procedure, in the framework of which it was postulated that

$$\frac{1}{w}\int_{-w/2}^{w/2}dy\ \sin\Phi(x,y,t)\approx\sin\left\{\frac{1}{w}\int_{-w/2}^{w/2}dy\ \Phi(x,y,t)\right\}$$

and the two-dimensional problem was reduced to an effective one-dimensional one. We shall show below that an effective one-dimensional approach to the long overlap Josephson junction based on Eq. (25) is valid only for narrow enough junctions ($w\leqslant 2$), while our approach based on the set of Eqs. (22) and (23) gives a good agreement with the results of two-dimensional numerical simulations in the whole interval for the width $0<w<2\pi$, and the SFM offers the possibility to extend to larger widths by including more terms from the expansion in (14).

III. STATIC SOLUTIONS IN THE OVERLAP GEOMETRY

The static properties of the junction are described by the solutions of Eqs. (22)–(24) when the time derivatives are neglected so that $A_0(x)$ and $A_1(x)$ are functions of x only. Denoting derivation with x by a prime we have

$$A_0''=C_0\sin A_0+S_0\cos A_0+(C_1\cos A_0-S_1\sin A_0)A_1-\frac{1}{2}(C_2\sin A_0+S_2\cos A_0)A_1^2-S_0, \quad (26)$$

$$A_1''=\left(\frac{2\pi}{w}\right)^2A_1+2[C_1\sin A_0+S_1\cos A_0+(C_2\cos A_0-S_2\sin A_0)A_1-S_1], \quad (27)$$

under the boundary conditions

$$A_0'(\pm\ell/2)=\mathcal{H}_e, \quad (28a)$$

$$A_1'(\pm\ell/2)=0. \quad (28b)$$

It is seen from Eqs. (26) and (27) that the longitudinal properties of the junction described by the amplitudes $A_0(x)$ and $A_1(x)$ depend on the coefficients C_n and S_n, which are determined by the transversal characteristics of the junction. Equation (26) reduces to the effective 1D model [11] if we set $A_1=0$, $C_0=1$, and neglect the term $S_0\cos A_0$.

When there is no external magnetic field ($\mathcal{H}_e=0$) Eqs. (26) and (27) have a trivial solution $A_0=A_1=0$. In this case the problem is reduced to the 1D one and the current and magnetic field distributions are described by Eqs. (8) and (9). The maximum current that goes through the barrier can be obtained from Eq. (10). In the interval of widths under consideration ($w\leqslant 2\pi$) the function $\mathrm{sd}((w/2)|m)$ is positive and for any m in the interval $[0,1]$ the current $\mathcal{I}$ is a nonmonotonic function of the modulus m with a single maximum at m^*. The position of m^* depends on the width of the junction. When $w\leqslant 2$, $m^*\approx\frac{1}{2}$ and $I_{\max}(\mathcal{H}_e=0)=\ell w$. When w is near 2π we have $m^*=8(\cosh^2w+16\cosh w)^{-1/2}$ and $I_{\max}(\mathcal{H}_e=0)=4\ell$.

For finite $\mathcal{H}_e$ we must also solve the set of Eqs. (26) and (27) with the boundary conditions (28). In the framework of our approach, the reason the maximum current which flows through the barrier depends on the external magnetic field $\mathcal{H}_e$ can be clarified if we consider simultaneously both equations for $\Phi_0(y)$ and $A_0(x)$ neglecting for simplicity $A_1(x)$. The external current $\mathcal{I}$ determines $\Phi_0(x)$ through its boundary condition (10) in which the external magnetic field $\mathcal{H}_e$ does not enter directly. It enters, however, in the equation for A_0 whose solution is not guaranteed for any external current, but for a given magnetic field $\mathcal{H}_e\neq 0$. Equation (26) gives a stable solution only up to a maximum value in the external current which depends on the external magnetic field. The

variation of $I_{\max}$ near $\mathcal{H}_e \approx 0$ with the external magnetic field can be estimated for narrow junctions ($w<2$). For small $\mathcal{H}_e$ the amplitude $A_0(x)$ is expected to be small and $A_1(x) \ll A_0(x)$. Therefore we can set $A_1(x)=0$, and, expanding the trigonometric functions in Eq. (30), we can write a simple equation for $A_0(x)$ which can be solved analytically. Using some analytic techniques we obtain the inequality (see Appendix A)

$$\mathcal{I}^2 \leqslant I_{\max}^2(\mathcal{H}_e=0)\left[1-\left(\frac{\mathcal{I}\mathcal{H}_e}{\ell w}\right)^{4/3}\right]. \tag{29}$$

Thus at finite $\mathcal{H}_e$ the maximum current will decrease with increasing magnetic field. An analytic solution of Eqs. (26)–(28) for a general $\mathcal{H}_e$ cannot be obtained. The above procedure shows that for small w and $\mathcal{H}_e$ the amplitude A_1 can be neglected, because as seen from Eq. (27) $A_1 \sim w^2 C_1 A_0$, and the contribution of A_1 to the equation for A_0 is $\sim w^2 C_1^2 A_0 \ll C_0 A_0$. For large w, one must solve the set of Eqs. (26)–(28) numerically as presented below along with a comparison with the results of two-dimensional numerical simulations.

IV. FLUX CONTENT OF 2D SOLUTIONS

In a 1D junction (very narrow and in-line boundary conditions) the magnetic flux can be characterized by the fluxon content (in units of the basic quantum of flux $\phi_0 = h/2e$), which increases with the magnetic field. Due to the sinusoidal nonlinearity of the Josephson term in the sine-Gordon equation the magnetic flux is a multiple valued function of the external magnetic field [1]. For a very short junction, where one obtains the characteristic Fraunhofer pattern for the maximum tunneling current, $I_{\max}(\mathcal{H}_e)$ is a single valued function where the maximum current vanishes when exactly a multiple number of flux quanta penetrate the junction along and normal to the long dimension. This creates a sequence of branches labeled $(n \to n+1)$ branches, signifying that the magnetic flux content is between n and $n+1$ fluxons. At the same time the maximum tunneling current (due to nonlinearity) is a nonmonotonic function of the external magnetic field. For a long junction there is an overlap between the different branches.

For a 2D junction, even when the external field is along one dimension, the magnetic field pattern is not one dimensional, so that it is necessary to define the flux penetration along both dimensions. Thus according to Eq. (3) the effective magnetic field $\vec{\mathcal{H}}$ is a two-dimensional vector in the plane of the barrier

$$\vec{\mathcal{H}} = (\partial_y \Phi, -\partial_x \Phi, 0). \tag{30}$$

The magnetic fluxes in units of the quantum of flux ϕ_0 that penetrate the junction along the two directions are

$$N_x = \frac{1}{2\pi d}\int_{-w/2}^{w/2} dy \int_{-d/2}^{d/2} dz\ H_x = \frac{1}{2\pi}\int_{-w/2}^{w/2} dy\ \partial_y \Phi$$
$$= \frac{1}{2\pi}\left[\Phi\left(x, \frac{w}{2}\right) - \Phi\left(x, -\frac{w}{2}\right)\right] \tag{31a}$$

and

$$N_y = \frac{1}{2\pi d}\int_{-\ell/2}^{\ell/2} dx \int_{-d/2}^{d/2} dz\ H_y = \frac{1}{2\pi}\int_{-\ell/2}^{\ell/2} dx\ \partial_x \Phi$$
$$= \frac{1}{2\pi}\left[\Phi\left(\frac{\ell}{2}, y\right) - \Phi\left(-\frac{\ell}{2}, y\right)\right]. \tag{31b}$$

Note that the fluxon content N_x is a function of x and N_y is a function of y.

We should remark that due to the boundary conditions considered here, the function $\Phi(x,y)$ is a symmetric function of y so that $N_x = 0$. If one neglects the term with A_1 then N_y is independent of y. This is the case when $w<2$ even though the field is two dimensional. In that case we have an effective separation of the x and y dependencies in the function $\Phi(x,y) = \Phi_0(y) + A_0(x)$. If, however, higher terms are needed in the expansion of (13), then the y-direction fluxon content is a function of y.

V. NUMERICAL RESULTS

The numerical solution of our quasi-one-dimensional model can be divided into two separate problems. The first involves the determination of $\Phi_0(y)$ from Eqs. (6) and (7) following the procedure in [6]. It gives the dominant variation of $\Phi(x,y)$ in y, since it takes into account the external current which gives the gradient of the phase difference along y. The second step is the numerical solution of the set of coupled nonlinear equations (26) and (27) with (28) for the modal amplitudes A_0 and A_1. For the geometries considered here A_0 along with $\Phi_0(y)$ are sufficient to reproduce the spatial variation of $\Phi(x,y)$. The results can be compared with the direct numerical solution of the time independent form of Eq. (2) with the overlap boundary conditions (5). For this purpose we used the Newton iterative method

$$\nabla^2 \Phi^{(i)} - \cos(\Phi^{(i-1)})\Phi^{(i)} = \sin(\Phi^{(i-1)}) - \cos(\Phi^{(i-1)})\Phi^{(i-1)}, \tag{32}$$

which has been analyzed in detail in [15]. This algorithm converges quadratically so that the norm of the difference between two successive iterates goes to zero in about five iterations. The main difficulty in the procedure comes from the choice of the initial guess which should be close enough to the solution. To obtain the $I_{\max}(\mathcal{H}_e)$ curve, we have started from the well known situation where $\mathcal{H}_e$ is very small, and the solution is close to $\pi/2$ so that the current is close to the maximum. We have then increased the current up to the point where the iteration (32) does not converge and then proceeded to bisect between these values to find the critical current. The magnetic field is then increased, and using the solution for the previous value of $\mathcal{H}_e$ and $\mathcal{I}$, we find the maximum current for this value of $\mathcal{H}_e$ by stepping and bisecting. For this to work, it is essential that the steps in $\mathcal{I}$ and $\mathcal{H}$ are close and small, and we took them to be a few percent. The whole procedure was implemented very efficiently using the ELLPACK software [16]. The typical number of mesh points used was about 80×60 so that one iteration took about 5 s on an IBM RS 6000 and the whole 0-1 fluxon branch could be obtained in about 12 h CPU time.

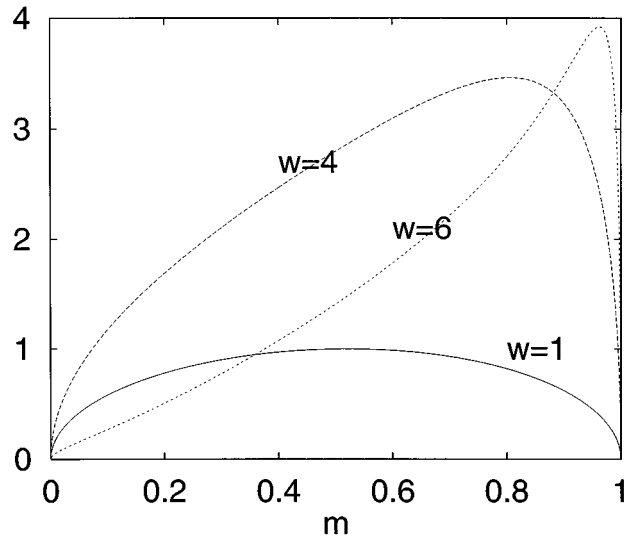

FIG. 2. $\mathcal{I}(m)$ from the left-hand side of Eq. (10) for three values of $w=1,4,6$.

The one-dimensional static sine-Gordon Eq. (6) and the equations for the modal amplitudes (A_0,A_1) were solved using MATLAB following the same approach, except that for the latter a bisection on m was used for large currents (near $\mathcal{H}_e\approx 0$) because of the difficulty in inverting Eq. (10). The number of mesh points was chosen to be 150 and the current tolerance for the bisection 10^{-2}.

In the SFM method the solution for $\Phi_0(y)$ is given in the form of elliptic functions with the modulus m $(0<m<1)$, which is determined from the boundary condition (10) for the external bias current. In general, this equation for a given $\mathcal{I}$ must be solved numerically. The left-hand side of (10) as a function of m depends strongly on the junction width w, as is seen in Fig. 2. For the values of w considered here $\mathcal{I}(m)$ has a single maximum at $m=m^*$ and for a given bias current there are two possible values in m that satisfy (10). From these only the one at the right of m^* corresponds to a stable solution. Here we should remark that, when we neglect the x dependence, all $m\geqslant m^*$ give stable solutions, and for a finite magnetic field this interval is reduced to $m>m_1>m^*$ as discussed above. To the value of m_1 corresponds the maximum possible current for the particular value of the external magnetic field. As seen in Fig. 2, for large w (but $w<2\pi$) the part of the curve above m^* becomes very steep near $m\approx 1$ so that the elliptic functions become hyperbolic-like. The class of solutions for $\Phi_0(y)$ has zero fluxon content, and is at the beginning of the $(0\rightarrow 1)$ branch, since in (10) no magnetic field is included. We mention that for even larger w [where more modal terms in (14) are needed] the function $\mathcal{I}(m)$ becomes oscillating with more maxima, but still only the region to the right of the last maximum very close to $m\approx 1$ is physically relevant.

Once m is determined and using the expression for $\Phi_0(y)$ we can evaluate the coefficients C_n and S_n which enter in the ODE's for $A_0(x)$ and $A_1(x)$. Thus the approximation to $\Phi(x,y)$ is obtained numerically. In Fig. 3 we plot, for a junction width of $w=1$, the constant phase lines for values of $\mathcal{I}$ corresponding to the maximum possible bias current at three values of $\mathcal{H}_e=0.1,1.0,1.9$ correspondingly. In

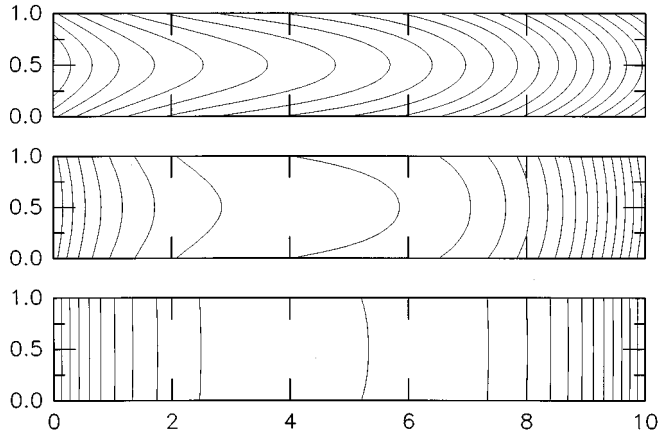

FIG. 3. Contour plots for the phase $\Phi(x,y)$ for a junction with $\ell=10$, $w=1$, and three values of (a) $\mathcal{H}_e=0.1$ (top), (b) 0.9 (middle), (c) 1.9 (bottom).

this and the following calculations the junction length is $\ell=10$. The top pattern is for $\mathcal{H}_e=0.1$ with $I_{\max}$ near its maximum (at $\mathcal{H}_e=0$). Increasing $\mathcal{H}_e$ causes the junction to act as a nonuniform barrier due to applied or internal current magnetic field penetration. This is reflected in the decreased curvature as we go down in Fig. 3 from (a) to (c). In Fig. 3(a) the phase is centered around $\Phi=\pi/2$, ranging from 1 in the center of the left edge to 1.95 at the corners of the right edge, so that $\sin\Phi$ is significant. The phase change along a fixed y value is about 0.7, implying a fluxon content $N_y\approx 0.1$ which is independent of y and is small as expected. In Fig. 3(b) for the increased $\mathcal{H}_e=1.0$ we introduced almost half a fluxon with $N_y=0.42$. Notice that the constant phase line spacing is different in the three figures 0.039 in (a), 0.122 in (b), and 0.225 in (c). In Fig. 3(c) the $\mathcal{I}$ (the maximum for $\mathcal{H}_e=1.9$) is very small since we have introduced almost one fluxon with $N_y=0.8$. At $\mathcal{H}_e=2$ the solution is the same as for the 1D in-line geometry since $I_{\max}(\mathcal{H}_e=0)=0$ and a whole fluxon has penetrated the junction.

In Fig. 4 we study the effect of the junction width $w=4,6,10$ on the phase pattern at a constant external magnetic field $\mathcal{H}_e=1$. In all three cases the contour spacing is fixed at $\Delta\Phi=0.167$. Thus taking into account the scaling of

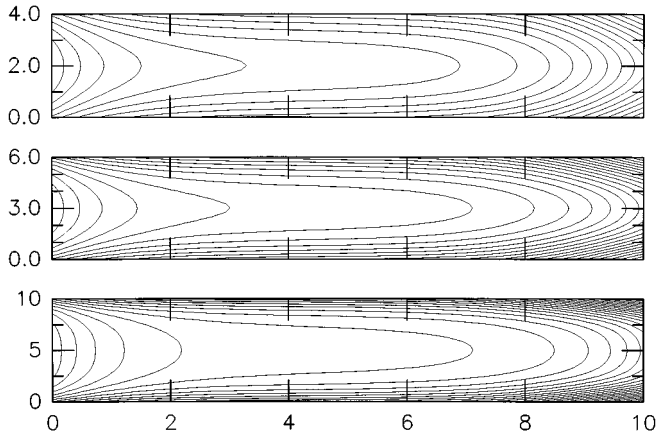

FIG. 4. Contour plots for the phase $\Phi(x,y)$ for a junction with $\ell=10$, $\mathcal{H}_e=1$, and three values of (a) $w=4$ (top), (b) 6 (middle), (c) 10 (bottom).

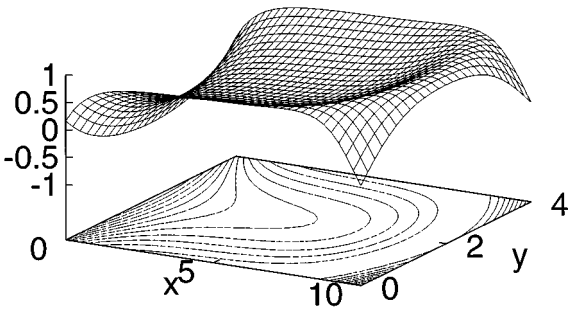

FIG. 5. 3D plot of the tunneling current distribution $\sin\Phi(x,y)$ for $\mathcal{H}_e=1$ and $w=4$.

the junction dimensions we see that the gradient along y is slightly increasing as we go from (a) to (c), implying a slightly higher current. In the center there is a relatively large area where the phase is slowly varying near $\Phi\approx 0$ since for weak fields the penetration is along the perimeter. The minimum of the phase is at the center of the left edge while the maximum is at the right edge corners where there are strong variations in the phase since the external magnetic field and bias current act additively. A clearer indication of this is in Fig. 5, where we give a 3D plot of the tunneling current distribution along the barrier interface. The fluxon content for the three curves is $N_y=0.36,0.4,0.46$ correspondingly reflecting the small increase in the maximum current.

In Fig. 6 we plot the functions $\Phi_0(y)$, $A_0(x)$, and $A_1(x)$ for a junction of width $w=4$ and three values of the external magnetic field $\mathcal{H}_e=0.1,1.0,1.95$. The current is chosen at its maximum value for the corresponding external field. The fluxon content N_y is essentially determined from A_0 and we see that it changes from $N_y=0.1,0.5,0.98$. Notice that the scale for A_1 is enlarged by a factor of 20. Thus in all three cases A_1 is small and the fluxon content can only weakly depend on y. For the case $\mathcal{H}_e=1.95$ we see that the function $\Phi_0(y)$ along with $A_1(x)$ almost vanish (they are zero for $\mathcal{H}_e=2.0$). The solution for the phase is simply $A_0(x)$ being clearly 1D since the current is near zero. At $\mathcal{H}_e=0.1$ the modal amplitudes are quite small, as expected.

In Fig. 7 we compare the phase line pattern (with fixed contour levels as in Fig. 4) for the case $\mathcal{H}_e=1$ [top plot Fig. 3(a)] using the 2D solution and that obtained from the SFM method by setting $A_1=0$ in Eq. (26) (top figure), and with A_1 included (bottom) in Eqs. (26) and (27). The basic structure is the same in all three cases, with only minor differences, which are compounded by the contour fitting procedure. The main difference is in the right edge of the junction where the phase varies significantly and the term A_1 should be included. The plot including both modal amplitudes is in good agreement with that obtained with the direct numerical solution of the 2D problem.

In Fig. 8 we plot the maximum tunneling current as a function of $\mathcal{H}_e$ for five values of junction width $w=1,2,3,4,6$. The solid line is the result of the direct solu-

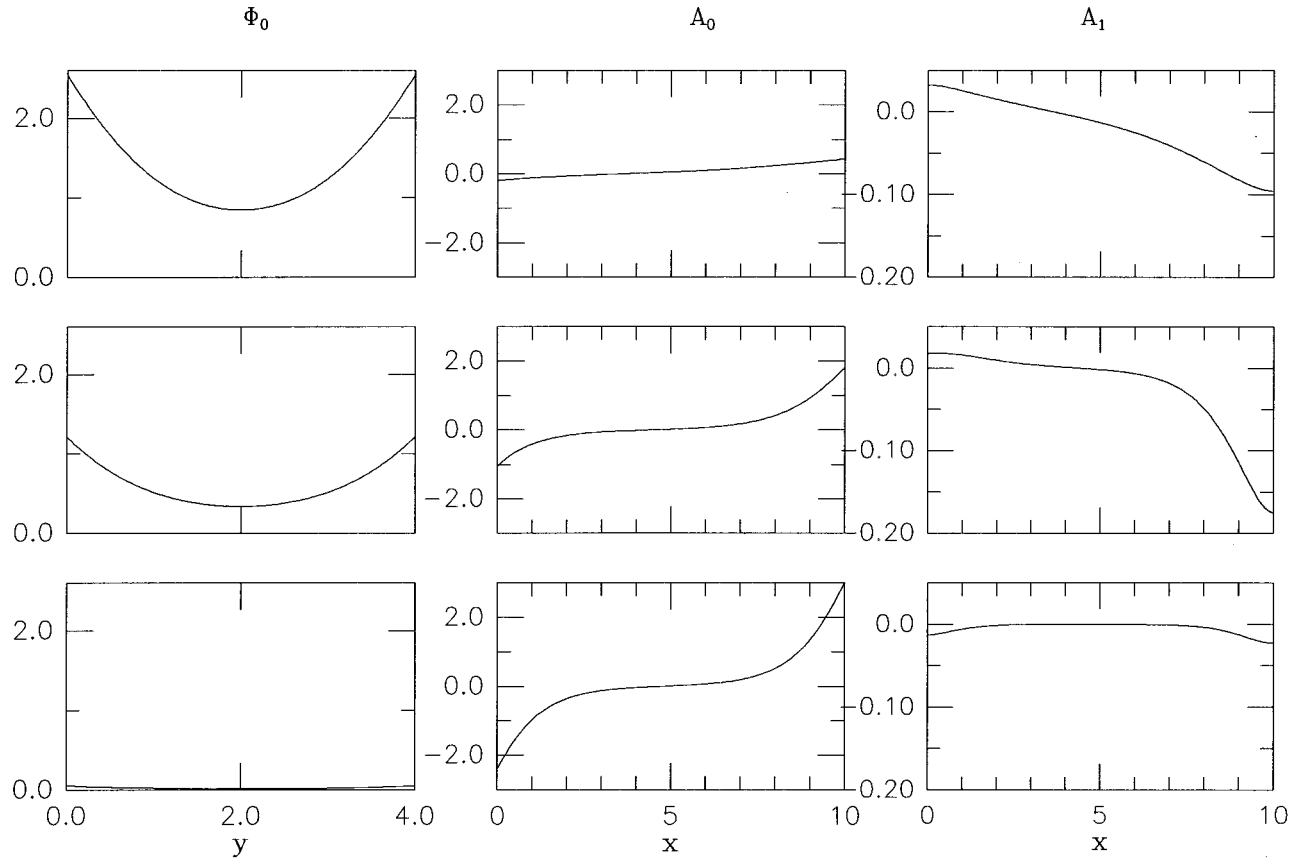

FIG. 6. Plots of the functions $\Phi_0(y)$ (left), $A_0(x)$ (middle), and $A_1(x)$ (right) for a wide junction $w=4$ and (a) $\mathcal{H}_e=0.1$ (top), (b) 1(middle), (c) 2 (bottom).

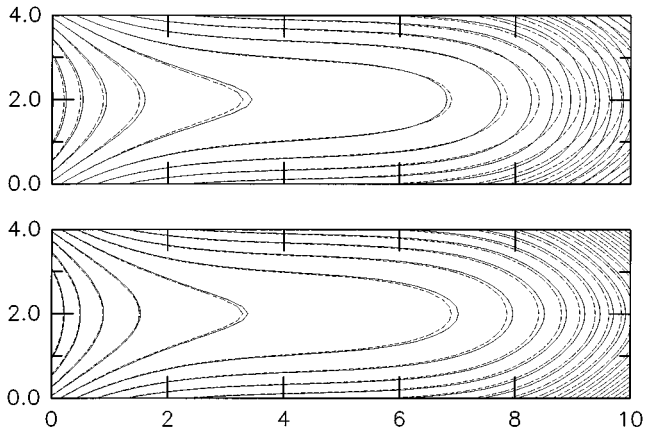

FIG. 7. Comparison of the contour plots for $\Phi(y)$ in a wide junction $w=4$ with $\mathcal{H}_e=1$ without the mode $A_1(x)$ (top) and including it (bottom). In both figures the dashed lines are the direct solution of the 2D sine-Gordon equation.

tion of the 2D sine-Gordon equation using ELLPACK. The dashed lines are the results of the 1D model as discussed in [11] and the points (different symbols for each w) are the results of our SFM model. We see that all three models give almost identical results for $w=1$ and $w=2$, implying that the use of the 1D model is adequate. Again all three models are in good agreement for all w near the right end of the $(0\rightarrow 1)$ branch, where the slope increases linearly with w. This is due to the vanishing of the maximum current and the boundary conditions are in line (1D), and near $\mathcal{H}_e=2$ it is the external magnetic field that dominates the pattern and its effect will be proportional to the junction width. The 1D model, however, deviates significantly from $w=3$ and on, especially near $\mathcal{H}_e=0$. This is the point, though, where our method gives the exact result, since at $\mathcal{H}_e=0$ we have $A_0=A_1=0$, and the current enters as in-line boundary condition along the y direction, which gives our function $\Phi_0(y)$. In fact, up to $w=4$ the SFM gives accurate results, and in fact the accuracy is not changed much if we neglect A_1. The approach deviates only slightly even for the relatively large $w=6$, above which higher modes may have to be included. For larger w the maximum current saturates in analogy with the corresponding effect in the 1D case [6]. We must stress that the significantly improved accuracy is obtained at no extra computational cost from the 1D model, especially when A_0 is sufficient to describe the spatial pattern. Of course the inclusion of A_1 automatically checks the convergence. Actually it can be seen from Eqs. (26) and (27) that A_1 enters as the square in the equation for A_0 with a small coefficient in front of it, while from (27) it is seen that it is important only if $w/2\pi \gg 1$. It was verified that using only A_0 changes the $I_{\max}$ slightly for $w \leqslant 3$.

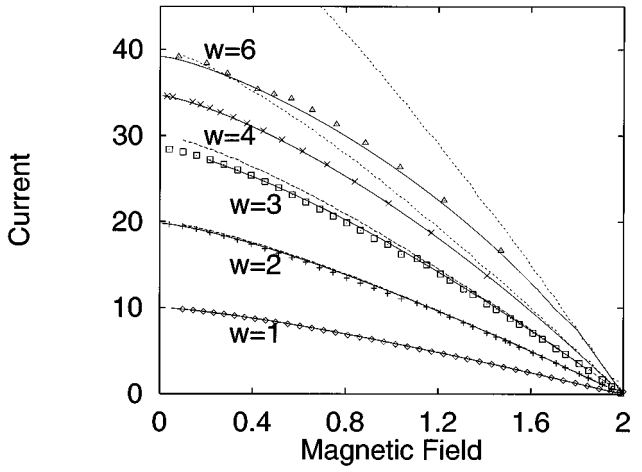

FIG. 8. Plot of the maximum tunneling current $I_{\max}$ vs the external magnetic field $\mathcal{H}_e$ for $w=1,2,3,4,6$. The solid lines are the direct solution of the static 2D sine-Gordon equation. The dashed line is the effective 1D model and the points (various symbols) are the results of the SFM method.

VI. CONCLUDING REMARKS

In this paper we developed a split Fourier mode method to study the static and dynamic properties of large area Josephson junctions with overlap boundary conditions. The method relies on separating out of the phase field the part $\Phi_0(y)$ that satisfies the external current boundary conditions. The rest is expanded in a Fourier series in y with the proper symmetry, whose dominant term $A_0(x)$ is y independent. The coupling between the x and y directions is included in a systematic way, but for the dimensions considered the first two terms in the expansion are sufficient. We explicitly demonstrated how the bias current enters as a driving term in the effective 1D model that was introduced intuitively in [17]. We performed numerical calculations using the SFM and the direct solution of the 2D problem and demonstrated that the effective 1D model is a good approximation for $w \leqslant 2$ while our model with only two terms is quite accurate at least up to $w=6$, reproducing not only global properties but also the complicated two-dimensional pattern. In this paper we concentrated on the first branch with (0,1) fluxon content where the 2D effects are strongest. The other branches that correspond to higher magnetic field with low bias currents are almost 1D-like. Some difference is of course expected in the peaks of the other branches.

For the first branch the commonly used 1D model gives a reasonable agreement up to $w=2$ while there are noticeable differences in the $I_{\max}$ for $w>3$. We also see a saturation effect with increasing w (near $w=6$) which is related to the similar effect in [6] at zero external magnetic field. In fact, the upper value of $I_{\max}$ at $H_e=0$ is easily obtained since we have in-line boundary conditions along y, and the lowest point (with $I_{\max}=0$ and $H_e=2$) satisfies in-line boundary conditions along x.

We introduced the notion of fluxon content in the x or y direction, which corresponds to the magnetic flux through the boundaries normal to the x or y direction and is a function of y and x correspondingly. For the boundary conditions considered $N_x=0$ and N_y is the equivalent of the fluxon content in 1D for a long junction. Here, however, it is slightly dependent on y for $w>3$ due to the internal self-magnetic-field.

The above calculations can be of relevance to direct measurements of the Josephson supercurrent distribution in large area tunneling junctions by means of low temperature scanning electron microscopy (LTSEM) [18]. It is very easy to reproduce also the boundary conditions and the form of criti-

cal current inhomogeneity to fit a particular experimental design. On the other hand, the maximum current at a given $\mathcal{H}_e$ is a quantity of interest for design purposes. The effect of the width on the dynamical behavior of the large area junction under a bias current and damping due to quasiparticle tunneling is currently being investigated. This will be reflected in the *I-V* characteristics.

ACKNOWLEDGMENTS

Part of this work was supported by EEC Grant No. SC1*–CT91–0760 and PENED Grants No. ED 479 and No. 2028(96) from the Greek Ministry of Research. Y.G. and J.G.C. acknowledge the hospitality of the University of Crete. The visit of Y.G. was made possible by a NATO grant from the Greek Ministry of Economy and that of J.G.C. by a grant under the Greek-French collaboration agreement. Y.G. received partial support from Grant No. K59100 of the International Science Foundation, the Government of Ukraine, and from SRC QM ''Vidhuk.''

APPENDIX

The variation of $I_{\max}$ near $\mathcal{H}_e \approx 0$ with the external magnetic field can be estimated for narrow junctions ($w<2$). For small $\mathcal{H}_e$ the amplitude $A_0(x)$ is expected to be small and $A_1(x) \ll A_0(x)$. Therefore we can put $A_1(x)=0$, and expanding the trigonometric functions in Eq. (26), we can write the equation for $A_0(x)$ in the form

$$A_0'' = C_0 A_0 - \frac{S_0}{2} A_0^2, \tag{A1}$$

with the boundary condition

$$A_0'(\pm \ell/2) = \mathcal{H}_e . \tag{A2}$$

Inserting Eq. (8) into (19) we get

$$S_0 = \frac{\mathcal{I}}{\ell w}. \tag{A3}$$

The coefficient C_0, which is defined by Eq. (21), has a much more complicated expression, but for narrow junctions it simplifies and can be written as follows:

$$C_0 \approx 1 - 2m_1 \approx \sqrt{1 - \frac{\mathcal{I}^2}{I_{\max}^2(\mathcal{H}_e=0)}}. \tag{A4}$$

The solution of Eq. (A1) can be represented in the form

$$A_0 = \frac{C_0}{S_0}\left\{1 - \frac{1}{\sqrt{q^2-q+1}}\left[2q-1+3q(1-q)\mathrm{cn}^2\left(\frac{\sqrt{C_0}}{2}\frac{x+x_0}{(q^2-q+1)^{1/4}}\middle| q\right)\right]\right\}, \tag{A5}$$

where the modulus q and the parameter x_0 may be obtained from the boundary conditions (A2). Inserting Eq. (A5) into Eq. (A2) we get

$$\frac{1}{S_0}\frac{6q(1-q)C_0^{3/2}}{(q^2-q+1)^{1/4}} f(u_\pm) = \mathcal{H}_e , \tag{A6}$$

where the abbreviations

$$f(u) = \mathrm{sn}(u|q)\,\mathrm{cn}(u|q)\,\mathrm{dn}(u|q) \tag{A7}$$

and

$$u_\pm = \frac{\sqrt{C_0}}{2}\frac{x_0 \pm \frac{L}{2}}{(q^2-q+1)^{1/4}} \tag{A8}$$

were used. The function $f(u)$ is positive in the interval $[0,K(q)]$ and reaches a maximum at the point u_0 where

$$\mathrm{sn}^2(u_0|q) = \frac{1+q-\sqrt{q^2-q+1}}{3q}. \tag{A9}$$

Equation (A6) can have a solution if

$$\mathcal{H}_e \leqslant \frac{6q(1-q)C_0^{3/2}}{(q^2-q+1)^{3/4}} f(u_0|q)\frac{1}{S_0}. \tag{A10}$$

Inserting Eq. (A9) into Eq. (A7) we find that

$$\frac{6q(1-q)}{(q^2-q+1)^{3/4}} f(u_0|q) = \frac{2}{\sqrt{3}}(1-q),$$

$$\left(1 - \frac{1-2q}{\sqrt{q^2-q+1}}\right)^{1/2}\left(1 + \frac{2-q}{\sqrt{q^2-q+1}}\right)^{1/2} \times \left(\frac{1+q}{\sqrt{q^2-q+1}} - 1\right)^{1/2} \equiv f_0(q). \tag{A11}$$

The function $f_0(q)$ becomes equal to zero at $q=0,1$ and has a maximum at some point $q=q^*$. Thus from Eq. (A10) we obtain that

$$\frac{1}{S_0} f_0(q^*) C_0^{3/2} \geqslant \mathcal{H}_e . \tag{A12}$$

Introducing Eqs. (A3) and (A4) in the inequality (A12) we see that

$$\mathcal{I}^2 \leqslant I_{\max}^2(\mathcal{H}_e=0)\left[1 - \left(\frac{\mathcal{I}\mathcal{H}_e}{\ell w}\right)^{4/3}\right]. \tag{A13}$$

[1] A. Barone and G. Paterno, *Physics and Applications of the Josephson Effect* (John Wiley, New York, 1982).
[2] J. M. Rowell, Phys. Rev. Lett. **11**, 200 (1963).
[3] R. C. Dynes and T. A. Fulton, Phys. Rev. B **3**, 3015 (1971).
[4] E. P. Balsamo, G. Paterno, A. Barone, M. Russo, and R. Vaglio, Phys. Status Solidi A **35**, K173 (1976).
[5] A. M. Goldman and P. J. Kreisman, Phys. Rev. **164**, 544 (1969).
[6] C. S. Owen and D. Scalapino, Phys. Rev. **164**, 538 (1967).
[7] J. Matisoo, J. Appl. Phys. **40**, 1813 (1969).
[8] K. Schwidtal, Phys. Rev. B **2**, 2526 (1970).
[9] A. Barone, W. J. Johnson, and R. Vaglio, J. Appl. Phys. **46**, 3628 (1975).
[10] R. Vaglio, J. Low Temp. Phys. **25**, 299 (1976).
[11] S. Pagano, B. Ruggiero, and E. Sarnelli, Phys. Rev. B **43**, 5364 (1991).
[12] *Handbook of Mathematical Functions*, edited by M. Abramowitz and I. A. Stegun (Dover Publications, Inc., New York, 1972).
[13] J. C. Eilbeck, P. S. Lomdahl, O. H. Olsen, and M. R. Samuelsen, J. Appl. Phys. **57**, 861 (1985).
[14] S. Pagano, C. Nappi, R. Cristiano, E. Esposito, L. Frunzio, L. Parlato, G. Peluso, G. Pepe, and U. Scotti di Uccio, in *Nonlinear Superconducting Devices and High-t_c Materials*, edited by R. D. Parmentier and N. F. Pedersen (World Scientific, Singapore, 1995), p. 437.
[15] J. G. Caputo, N. Flytzanis, and E. Vavalis, Int. J. Mod. Phys. C **6**, 241 (1995).
[16] J. Rice and R. Boisvert, *Solving Elliptic Problems Using ELLPACK* (Springer-Verlag, Berlin, 1985).
[17] A. C. Scott, *Active and Nonlinear Wave Propagation in Electronics* (Wiley-Interscience, New York, 1970).
[18] J. Mannhart, J. Bosch, R. Gross, and R. P. Huebener, Phys. Lett. A **121**, 241 (1987).